Journal of Biomolecular NMR, **16:** 183–196, 2000.
KLUWER/ESCOM

The influence of DNA binding on the backbone dynamics of the yeast cell-cycle protein Mbp1*

Pauline B. McIntosh[a], Ian A. Taylor[b], Thomas A. Frenkiel[c], Stephen J. Smerdon[b] & Andrew N. Lane[a,**]
[a]*Division of Molecular Structure,* [b]*Division of Protein Structure, and* [c]*Biomedical NMR Centre, National Institute for Medical Research, The Ridgeway, Mill Hill, London NW7 1AA, U.K.*

Received 11 November 1999; Accepted 12 January 2000

Key words: backbone dynamics, chemical exchange, Mbp1-DNA interaction, spectral density mapping

Abstract

Mbp1 is a transcription factor involved in the regulation of the cell cycle in yeast. The N-terminus of this protein contains a DNA binding domain that includes a winged helix-turn-helix motif. The C-terminal 24 residues of this domain (the 'tail') are disordered in the crystal state, but are important for DNA binding. We have measured ^{15}N NMR relaxation rates at 11.75 and 14.1 T to determine the dynamics of the free protein and in its complex with a specific DNA duplex. The dynamics data were quantitatively analysed using both spectral density mapping and the Lipari–Szabo formalism including the effects of chemical exchange and rotational anisotropy. A detailed analysis has been made of the effect of anisotropy, exchange and experimental precision on the recovered motional parameters. The backbone NH relaxation is affected by motions on a variety of time scales from millisecond to tens of picoseconds. The relaxation data show a structured core of 100 residues corresponding to that observed in the crystal state. Within the core of the protein, two regions on either side of the putative recognition helix (helix B) show slow (ca. 0.2 ms) conformational exchange dynamics that are quenched upon DNA binding. The C-terminal 24 residues are generally more dynamic than in the core. However, in the free protein, a stretch of ∼8 residues in the middle of the tail show relaxation behaviour similar to that in the core, indicating a structured region. NOEs between Ala 114 in this structured part of the tail and residues in the N-terminal beta strand of the core of the protein demonstrate that the tail folds back onto the core of the protein. In the complex with DNA, the structured part of the tail extends by ca. 3 residues. These data provide a framework for understanding the biochemical data on the mechanism and specificity of DNA binding.

Abbreviations: MBF, MCB binding factor; SBF, SCB binding factor; MCB, MluI cell cycle box; SCB, Swi4/6 cell cycle box; Mbp1, Mlu1 cell cycle box Binding Protein.

Introduction

Central to the control of entry into the cell cycle in *S. cerevisiae* are the start-specific multimeric transcriptional complexes MBF (MluI cell cycle box binding factor) and SBF (Swi4/6 cell cycle box binding factor). The Swi6 protein, common to both multimeric complexes, is required for transcriptional activation but possesses no intrinsic DNA binding activity. This activity is supplied by two related proteins, Swi4 and Mbp1 (Primig et al., 1992; Koch et al., 1993). Thus, heteromers of Swi6/Swi4 bind to upstream sequences in the cyclin promoters known as SCBs which exist in multiple copies and have the consensus sequence 5′-CACGAAA-3′ (Primig et al., 1992). Similarly, genes required for DNA replication are regulated by binding of Swi6/Mbp1 heteromers to sequences called MCBs with the consensus 5′-ACGCGTNA-3′

*This paper is dedicated to the memory of Jean-François Lefèvre, who died in March 1999.
**To whom correspondence should be addressed. E-mail: alane@nimr.mrc.ac.uk

(McIntosh et al., 1991). Homologous proteins have been identified in fission yeast: Cdc10, Res1/Sct1 and Res2/Pct1 share three regions of sequence similarity with their *S. cerevisiae* counterparts (Lowndes et al., 1992). The central region consists of a series of repeating sequences, known variously as Swi6/cdc10 or ankyrin motifs (Breeden and Nasmyth, 1987; Sedgwick et al., 1998; Foord et al., 1999). These sequences occur widely and are known to mediate a variety of protein–protein interactions in other systems (Bork, 1993; Sedgwick and Smerdon, 1999). A short region of around 100–150 residues at the C-termini of these proteins appears to be both necessary and sufficient for SBF and MBF assembly (Sidorova and Breeden, 1993). Finally, the highly conserved N-terminal regions of Swi4, Mbp1, Res1 and Res2 mediate the DNA-binding activities of these transcriptional complexes.

The structure of a 124-residue fragment from the N-terminus of Mbp1, Mbp1(124), which comprises the DNA binding domain, has been determined by X-ray crystallography (Taylor et al., 1997; Xu et al., 1997). In this structure, electron density was only observed for residues 3–100 and the remaining C-terminal 24 residues were disordered. It is not clear whether the disorder is dynamic or static due to crystal contacts. However, deletion analyses and proteolysis protection experiments have shown that residues within this C-terminal tail (101–124) are crucial for full DNA-binding activity (Taylor et al., 2000).

The secondary structure of free Mbp1(124) in solution, determined from chemical shift indices (Wishart et al., 1992, 1994) for Cα, Hα, Cβ (McIntosh et al., 1999) and C′ in conjunction with characteristic sequential (d_{NN}, $d_{\alpha N}$), medium ($d_{\alpha iNi+3}$) and long range NOEs, showed the same elements of secondary structure as defined in the X-ray structure, with only slight differences in the length of the most C-terminal helix (McIntosh et al., 1999). Furthermore, the NOE patterns and the Cα and Hα chemical shifts show that there is no significant difference in the location or extent of these secondary structure elements in the specific Mbp1(124):DNA complex (McIntosh et al., 1999).

The amide ^{1}H and ^{15}N chemical shifts of the free protein and in its complex with a specific 12 bp DNA duplex have previously been determined by triple-resonance NMR methods (McIntosh et al., 1999). These assignments enable us to use ^{15}N NMR relaxation measurements to investigate the dynamics of backbone N-H groups and to investigate the degree of order of the tail and its role in DNA binding. ^{15}N NMR relaxation measurements are generally useful for determining the amplitude and time scale of fast internal motions in the backbones of proteins, and for identifying regions of high mobility as well as residues that undergo slower conformational exchange (Daragan and Mayo, 1997; Fischer et al., 1998; Feher and Cavanagh, 1999). They have also been used to characterise the degree of rotational anisotropy of proteins (Barbato et al., 1992; Tjandra et al., 1995, 1997; Zheng et al., 1995) and to determine the orientation of secondary structure elements with respect to the principal axis of the rotational diffusion tensor (Broadhurst et al., 1995; Luginbühl et al., 1997). Changes in dynamics on forming a protein–ligand complex (DNA in the present context) can be related to a part of the binding entropy (Yang and Kay, 1996; Fischer et al., 1998).

Here we show that the C-terminal tail residues are dynamically disordered in solution, except for a short segment in the centre of the tail which folds back onto the N-terminal beta strand of the core. Formation of the specific protein:DNA complex results in an extension of the ordered portion of the tail, and quenching of slow conformational exchange processes in residues adjacent to the putative recognition helix. These data complement the X-ray crystallographic work (Taylor et al., 1997; Xu et al., 1997), and provide a framework for understanding the biochemical data on the mechanism and DNA binding specificity (Taylor et al., 2000).

Materials and methods

Materials

Unlabelled and isotopically labelled Mbp1(124) was produced using an *E. coli* expression system as previously described (Taylor and Smerdon, 1997; McIntosh et al., 1999).

Methods

Samples were made up for NMR spectroscopy in 40 mM Na-phosphate, 100 mM NaCl, pH 7.6 as previously described (McIntosh et al., 1999).

NMR spectra were recorded at 11.75 and 14.1 T at 288 K on Varian UnityPlus or Unity spectrometers, respectively. Heteronuclear ^{15}N-^{1}H NMR spectra were recorded using standard methods (Bodenhausen et al., 1980; Fesik and Zuiderweg, 1988). ^{15}N relaxation rate constants R_1, R_2, $R_{1\rho}$ and the ^{15}N{^{1}H} NOE were

obtained using standard methods (Kay et al., 1989, 1992; Peng and Wagner, 1992). In these sequences, repeated inversion of the ^{1}H resonances during the variable delay period was used to suppress the dipole-CSA cross-correlation effects (Kay et al., 1989; Boyd et al., 1990; Peng and Wagner, 1992). The values of R_1, $R_{1\rho}$ and R_2 were determined by least-squares fitting to a single exponential decay for each resolved peak, using peak volume as a function of delay time. The NOE spectra were recorded in interleaved mode, and the NOE calculated as the ratio of the peak volume with and without proton saturation. The relaxation delay in these experiments was 4.2 s (free protein) or 5 s (complex) corresponding to $>5T_1$. All relaxation experiments were carried out two or three times at each field strength.

The rotating frame relaxation measurements were used both to characterise exchange contributions (as described below), and, for non-exchanging residues, as an additional source of T_2 data. Thus, for the residues that showed no exchange the value of $R_{1\rho}$ is equal to R_2 when the spin-lock field is on resonance. When the spin-lock is not on resonance, $R_{1\rho}$ depends on the offset (Farmer et al., 1988; Davis et al., 1994):

$$R_{1\rho} = R_1 \sin^2 \psi + R_2 \cos^2 \psi \quad (1)$$

where ψ is the tilt angle, $\psi = \cos^{-1}(\omega_1/(\omega_1^2 + \Delta\omega^2)^{1/2})$, $\Delta\omega$ is the offset of a resonance from the carrier frequency and ω_1 is the radiofrequency field-strength (Davis et al., 1994). As the offset is known for each nitrogen resonance, R_2 can be calculated from Equation 1 together with the measured R_1 values. Because $R_{1\rho}$ was measured at different offsets and spin-lock strengths, good experimental statistics of the precision of R_2 can be determined for those residues for which there is no significant exchange contribution. The R_2 and $R_{1\rho}$ data at 14.1 T amounted to 12 independent estimations of R_2 with a standard deviation of 3–4% of the mean and maximum errors of up to 9–10%. We regard these experimental standard deviations as being more representative than those estimated from Monte Carlo sampling of single data sets (Press et al., 1986; Kördel et al., 1992). The values of R_2 were further checked by measuring the ^{15}N line-width in HSQC spectra recorded with proton decoupling and a long acquisition time (ca. 0.5 s) in the evolution period (Bax et al., 1990). Residual line-widths from imperfect proton decoupling and line broadening from magnetic field inhomogeneity were estimated as <0.5 Hz (ca. 1.5 s^{-1} for R_2).

Exchange contributions

In the rotating frame, the relaxation depends on both the dipolar and CSA mechanisms, and also on the exchange between two (or more) conformations as (Deverell et al., 1970):

$$R_{1\rho} = R_{1\rho}^0 + 4\pi^2 p_a(1 - p_a)\Delta\upsilon^2 k/(k^2 + \omega_1^2) \quad (2)$$

where $R_{1\rho}^0$ is the relaxation rate constant in the absence of exchange (when ω_1 is very large), p_a is the population of conformer A, $\Delta\upsilon$ is the chemical shift difference between the two conformational states, k is the exchange rate constant (equal to $k_1 + k_{-1}$) and ω_1 is the spin-lock field strength. Measurement of $R_{1\rho}$ at different values of ω_1 provides estimates of k and $4\pi^2 p_a(1-p_a)\Delta\upsilon^2$. The maximum value of $\Delta\upsilon$ is found for $p_a = 0.5$, so that a lower limit to $\Delta\upsilon$ can be calculated.

However, both terms in Equation 2 depend on the offset, as has been discussed in detail by Davis et al. (1994). At low spin-lock field strengths, offset effects on $R_{1\rho}$ can be large and the appropriate corrections cannot be made as the offsets (and other properties) of the individual conformers A and B are unknown. We have minimized the offset effects by using a CPMG pulse train to obtain values of $R_{1\rho}$ at low values of ω_1 ($\gamma B_1/2\pi < 0.5$ kHz), together with CW spin-locking experiments for $\gamma B_1/2\pi > 1$ kHz. The CPMG pulse train effectively spin-locks the magnetisation along the y-axis and under high pulse repetition rates the relaxation is equivalent to that of a CW spin-lock (Davis et al., 1994). To further minimise offset effects, the CW $R_{1\rho}$ experiments were carried out with the carrier at three different frequencies, such that the largest offset from the closest carrier position used was 200 Hz. This corresponds to a tilt-angle of 11° at $\gamma B_1/2\pi = 1$ kHz and 6° at $\gamma B_1/2\pi = 2$ kHz; these represent maximum errors from offset effects. For the CPMG experiments the effective spin-lock strength was calculated from the CPMG duty cycle and the width of the ^{15}N pulses (ca. 85 μs for a 180° pulse).

Modelling relaxation data

The relaxation data were first analysed using the model-free approach (Lipari and Szabo, 1982) assuming dipolar interactions with the attached proton, chemical shift anisotropy (CSA), and exchange are operative. Standard expressions for R_1, R_2 and the NOE were used (Clore et al., 1990; Barbato et al., 1992; Daragan and Mayo, 1997), with $r_{NH} = 1.02$ Å, and the anisotropy $\Delta\sigma = -170$ ppm.

For a non-spherical rotor the relaxation depends on the orientation of the N-H vector relative to the principal axis of the rotational diffusion tensor and more complex spectral density functions are needed for a full description (see below). However, for moderate degrees of anisotropy the simple spectral density function can provide a good fit to the measured relaxation data, with τ_0 a site-dependent parameter (Barbato et al., 1992; Schurr et al., 1994; Broadhurst et al., 1995). The program Relaxm (A.N. Lane, unpublished) was used to find optimal agreement with the relaxation data at each site using an exhaustive grid search for the rotational correlation time, the order parameter and the internal correlation time. The target function E for the grid search was:

$$E = (R_1 - R_1obs)^2 + (R_2 - R_2obs)^2 + (NOE - NOEobs)^2 \quad (3)$$

R_1, R_2, and the NOE were calculated with the omission of the exchange term from R_2. For each NH, the values of S^2, τ_0 and τ_e were found by searching over the ranges 0–1 in steps of 0.02 (S^2), 4–20 ns in steps of 0.08 ns (τ_0) and 0–0.2 ns in steps of 2 ps (τ_e) at both magnetic field strengths; 10^6 calculations of E (Equation 3) were carried out for each site.

Residues for which τ_0 was one or more standard deviations from the mean were excluded. These residues are either unusually mobile, or there are additional mechanisms contributing to the relaxation, such as chemical exchange. Where the R_2 values were substantially larger than the average, they were excluded and the R_1 and NOE values at 11.75 T and 14.1 T were simultaneously fitted. The difference between the predicted value of R_2 and the observed value was taken as an estimate of the exchange contribution, R_x. These calculated exchange contributions were compared to experimental values obtained from rotating-frame relaxation ($R_{1\rho}$) measurements.

Once an estimate of the exchange contribution had been obtained, the complete relaxation data were further analysed as a symmetric top rotor. The spectral density functions then depend on the angle, θ, between the NH vector and the principal axis of the diffusion tensor (Woessner, 1962; Schurr et al., 1994) and the two correlation times for rotation of the long, τ_L, and short, τ_s, axes, respectively. To account for rapid internal motions, the spectral densities were written as sums of terms as described by Schurr et al. (1994). Initial estimates of τ_L and τ_s were obtained from the largest and smallest values of τ_0 as described by Schurr et al. (1994) and Luginbühl et al. (1997). The overall fit to the experimental relaxation data was then optimised for a range of τ_L and anisotropies ($f = \tau_L/\tau_s$) by grid searching on S^2, θ and τ_e, with the exchange contribution fixed at the independently determined values. Thus $3n + 2$ parameters are to be determined (n = number of sites), from 6n observations (R_1, R_2 and NOE at two B_0 values). To evaluate the ability of the algorithm to obtain the various motional parameters, sets of simulated data including noise were analysed by the same procedure.

We have also used spectral density mapping for analysing ^{15}N relaxation data (Peng and Wagner, 1992; Farrow et al., 1995; Lefèvre et al., 1996; Fischer et al., 1998; van Heijenoort et al., 1998). In this method, the spectral densities at zero, ω_N and ω_H are determined from the relaxation rate constants, which requires no major prior assumptions about the dynamic behaviour and is therefore more truly model-free. The various spectral density profiles can be interpreted to provide information on flexibility or slow conformational exchange and to describe the anisotropic nature of the molecule (Lefèvre et al., 1996; van Heijneoort et al., 1998).

We have used the reduced spectral-density approach (Farrow et al., 1995; Lefèvre et al., 1996) with the assumption that $J(\omega)$ is proportional to $1/\omega^2$ for large ω; the three high-frequency spectral densities can then be related since $J(\Sigma\omega) = J(\omega_H)*(\omega_H/\Sigma\omega)^2 \cong 1.24J(\omega_H)$, and $J(\Delta\omega) = J(\omega_H)*(\omega_H/\Delta\omega)^2 \cong 0.82J(\omega_H)$. This gives:

$$J(\omega_H) = R_1(NOE - 1)(\gamma_N/\gamma_H)/(6.60\alpha/r^6) \quad (4)$$

$$J(0) = [R_2 - 0.5R_1 - 3(\alpha/r^6)J(\omega_H)]/[(2\alpha/r^6) + (2\beta/3)(\Delta\sigma)^2\omega_N^2] \quad (5)$$

$$J(\omega_N) = [R_1 - 8.25(\alpha/r^6)J(\omega_H)]/[(3\alpha/r^6) + \beta\omega_N^2(\Delta\sigma)^2] \quad (6)$$

For comparison with the model-free analysis, the resulting spectral densities were fitted to sums of Lorentzians according to:

$$J(\omega) = \Sigma a_i\tau_i/(1 + \omega^2\tau_i^2) \quad \text{with i = 1...n} \quad (7)$$

where a_i are amplitudes, with $\Sigma a_i = 1$ and τ_i are correlation times; n was varied from 1 to 3.

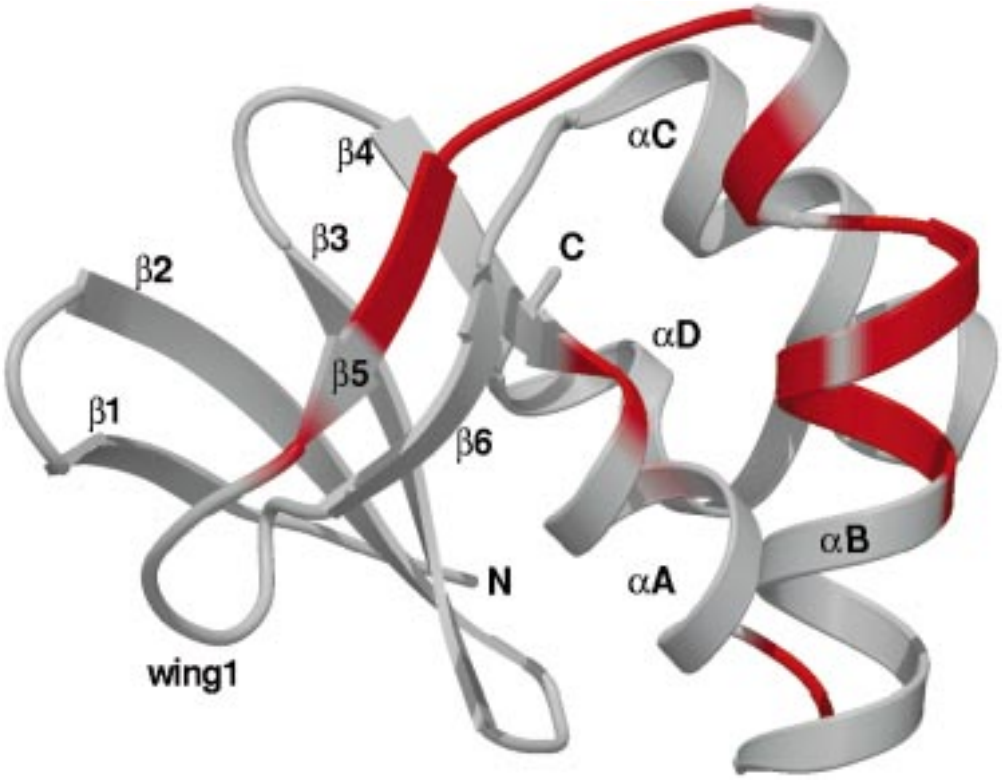

Figure 1. Ribbon diagram of the X-ray crystal structure of the DNA binding domain of Mbp1 generated using the MOLSCRIPT program (Kraulis, 1991). β Strands are labelled 1–6 and α helices A–D. Residues identified as having a conformational exchange contribution from the analysis of the ^{15}N NMR relaxation data are shown in red.

Results

^{15}N Relaxation behaviour of free Mbp1(124)

For simplicity, the Mbp1(124) fragment can be divided into two regions. We will refer to residues 3–100 as the 'core': they are ordered in the crystal structure and encompass the region of highest sequence homology (Taylor et al., 1997). The remaining 24 residues (101–124) will be referred to as the 'tail' of the molecule. A ribbon diagram of the core structure is shown in Figure 1.

We have determined the relaxation rate parameters R_1, R_2, NOE and $R_{1\rho}$ for each resolved and assigned backbone amide nitrogen in Mbp1(124) (see Methods). The relaxation rate constants R_1, R_2 and the NOE vary along the sequence of free Mbp1(124) (Figure 2). Within the core region, the relaxation data fall into two major classes. In the first class, residues 3–39, 46–55 and 65–100, the values of R_1, R_2 and NOE are fairly constant. For these residues, R_1 is about 30% smaller at 14.1 T than at 11.75 T, whereas R_2 is about 10% larger at 14.1 T. Furthermore, the value of $R_{1\rho}$ is equal to R_2 (and see below). These observations are typical for a folded, compact protein.

In the second class, residues 40 to 45 and 56 to 64, the R_2 values are much larger than those of the first class, while their R_1 and NOE values are similar to those of the first class. The R_2 values of the class two residues increase 30–40% between 11.75 T and 14.1 T and the values of $R_{1\rho}$ decrease with increasing spin-lock strength: at a spin-lock strength of 2.1 kHz the $R_{1\rho}$ values are similar to those of the class one residues in the core, which are in turn identical within experimental error to R_2 (and see below). The dependence of $R_{1\rho}$ on spin-lock field strength is characteristic of a chemical exchange process between two (or more) sites for which the exchange rate constant is larger than but comparable to the ^{15}N chemical shift difference in Hz (Deverell et al., 1970; Lane et al., 1993; Szyperski et al., 1993) (see below).

In the tail region, the relaxation data again fall into two classes. For residues 102–108 and 118–124 and the subsequent linker and hexahistidine tag, the NOE and R_2 are smaller than in the core, whereas

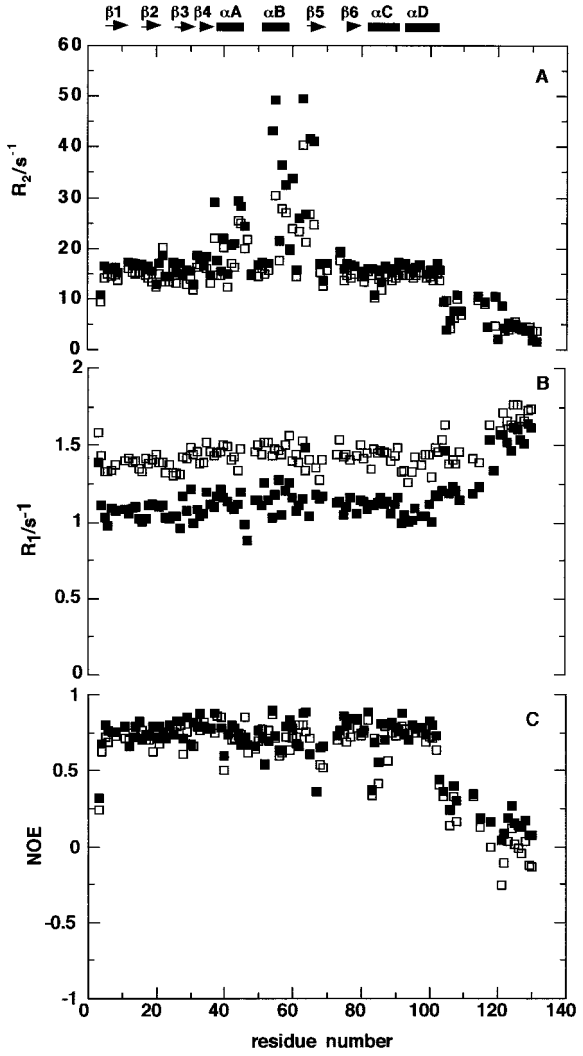

Figure 2. Relaxation rate constants in free Mbp1(124) at 288 K versus sequence number. ^{15}N relaxation rate constants were determined at 11.75 and 14.1 T as described in the text. The secondary structure elements determined from NMR data are shown at the top of the figure (see text). (A) R_2 at 14.1 T (■) and 11.75 T (□). (B) R_1 at 14.1 T (■) and 11.75 T (□). (C) NOE (■) at 14.1 T and (□)11.75 T.

R_1 is larger (Figure 2). This indicates the presence of large amplitude motions on the sub-nanosecond timescale. A more gradual change in the relaxation rate constants occurs from residue 118 onwards, which is typical of unstructured regions at chain termini (Levy et al., 1981) and is generally observed (Kördel et al., 1992; Broadhurst et al., 1995; Zheng et al., 1995; Wand et al., 1996). Indeed, for residue 120 and the residues onwards the relaxation rates are comparable to those observed for denatured proteins (Schwalbe et al., 1997) and are in agreement with these residues having random-coil shifts (McIntosh et al., 1999). In contrast, the values of the relaxation rate constants of residues 109–116 are intermediate between those of the core residues and the other tail residues. If the entire tail were essentially a random coil, then the relaxation rate constants from residue 102 onwards would monotonically approach those characteristic of a denatured protein. The observed pattern (Figure 2) is more typical of an exposed loop within a folded protein, where a few residues have lower NOEs and R_2 values than the residues in the structured regions on either side of them (Clore et al., 1990; Barbato et al., 1992; Kördel et al., 1992). Thus, the relaxation data suggest that there is a mobile loop between residues 102–108, followed by a structured region up to ca. residue 116, followed by essentially random coil.

Residues 109–116 have relaxation rate constants that are more similar to those of the core of the protein (Figure 2). This region includes a PPPAP sequence (111–115). Unfortunately, ^{15}N relaxation data is not obtained from the proline residues using the ^{1}H-detected ^{15}N-HSQC experiment. However, because the backbone torsion angle ϕ is restricted in proline, only part of the allowed region of Ramachandran space can be populated, and the oligoPro may adopt a polyPro-like helix part of the time. The core-like relaxation of residues 109–116 suggests that the peptide folds back onto the protein such that the correlation time of these residues becomes similar to that of the core of the protein. This has been confirmed by the observation of NOEs between Ala 114 NH and CH_3 and Ser 7 NH and Tyr 6 aromatic protons, as shown in the ^{15}N-edited NOESY-HSQC spectrum (Figure 3).

Chemical exchange in free Mbp1(124)

To analyse the relaxation data quantitatively, it is necessary to account for the exchange contribution to the spin-spin relaxation. Because the R_1 and NOE values observed for residues 40–45 and 56–64 are similar to those of the majority of the core residues, it is likely that the contributions from fast dynamics to R_2 should also be similar, i.e. those residues that undergo slow conformational exchange do not also have unusually large-amplitude sub-nanosecond motions.

The conformational exchange process was further analysed by measuring R_1 in the rotating frame ($R_{1\rho}$) as a function of spin-lock field strength, as described in the Methods. Figure 4 shows ^{15}N $R_{1\rho}$ dispersion curves for three of the residues that are in fast intermediate chemical exchange. k and $\Delta\upsilon_{app}$ were obtained

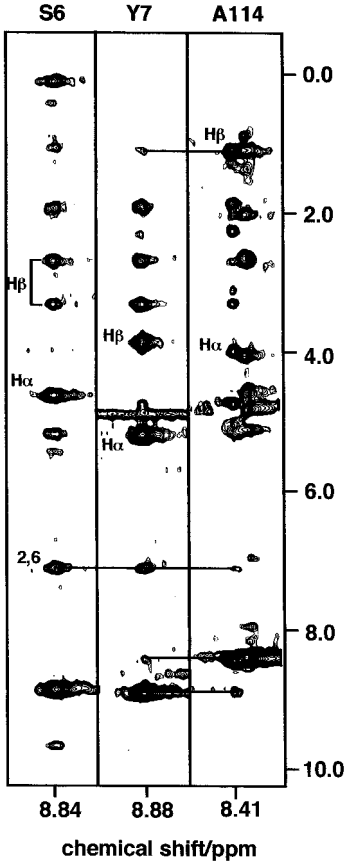

Figure 3. NOEs between protons of Ala 114 and Ser 6, Tyr 7 showing that the tail folds onto the core. Strips were taken from a 3D ^{15}N-edited NOESY-HSQC spectrum of Mbp1(124) recorded at 11.75 T and 288 K with a mixing time of 100 ms. The strips are taken at the ^{15}N shifts corresponding to the amide nitrogens of Tyr 6, Ser 7 and Ala 114, and demonstrate an interaction between the C-terminal tail and the core of the protein.

by fitting Equation 2 to the data. The precision of the $R_{1\rho}$ values for these broad peaks is lower than for those that do not show exchange. Furthermore, given the modest degree of sampling (Equation 2), the optimised values of k and $\Delta\upsilon_{app}$ are of only moderate precision. However, the values of k determined for these residues were in the range 5000–8000 s^{-1}, and the apparent frequency difference (assuming $p_a = 0.5$) was in the range 100–160 Hz at 14.1 T. Hence, this group of residues shows exchange on the time scale of ca. 0.2 ms, with shift differences of 1–2 ppm between the conformations being averaged. The exchange contribution found in this way was then used to correct the R_2 values for further analysis (see below).

The exchange contribution has been mapped onto the surface of the core protein (Figure 1). This shows

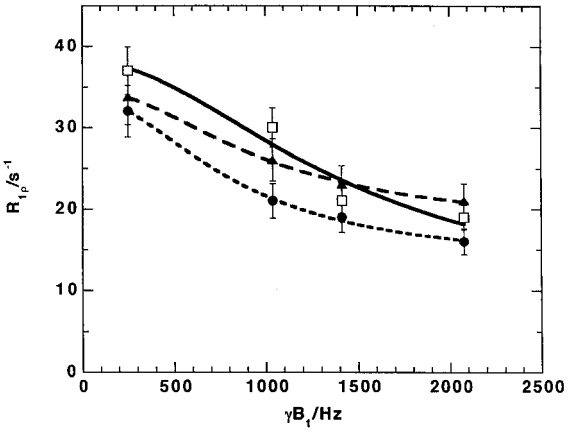

Figure 4. $R_{1\rho}$ dispersion curves for selected residues in free Mbp1(124) at 288 K. $R_{1\rho}$ was measured at 14.1 T using either a CW spin-lock or CPMG as described in the text. (□ —) Glu 55: $R^0_{1\rho} = 9\ s^{-1}$, $\Delta\upsilon_{app} = 162$ Hz, $k = 8900\ s^{-1}$; (● —) Lys 56: $R^0_{1\rho} = 13.4\ s^{-1}$, $\Delta\upsilon_{app} = 103$ Hz, $k = 5175\ s^{-1}$; (▲ —) Leu 59: $R^0_{1\rho} = 17.8\ s^{-1}$, $\Delta\upsilon_{app} = 103$ Hz, $k = 6190\ s^{-1}$. The curves are best fits to Equation 2.

that the exchange contribution lies over the expected DNA binding surface (helix B and adjacent loop) and coincides with an area of positive electrostatic potential and high crystallographic B values (Taylor et al., 1997).

Analysis of the relaxation data with the model-free approach (Lipari and Szabo, 1982)

The relaxation data were analysed using the Lipari–Szabo (1982) approach as described in the Methods. Values of the site correlation time, order parameter and internal correlation time were determined for each N-H vector for the relaxation data measured at 11.75 T and 14.1 T, both separately and together. The Lipari–Szabo parameters were also determined for the residues that showed exchange effects by excluding the R_2 values for these residues, using the experimental R_1 and NOE at both magnetic field strengths. These data were then further analysed using the R_2 values corrected for the exchange contribution as described below. Excellent agreement was obtained between the parameters derived from the relaxation data obtained at 11.75 or 14.1 T.

The average of the site correlation times obtained for the core residues of the protein from this analysis was 12.1±0.7 ns at 15 °C (residues 4–100) (see Table 1). This is typical for a protein of this size (Daragan and Mayo, 1997), indicating that it remains monomeric at millimolar concentrations. The

Table 1. Statistics of relaxation parameters

Parameter	Dimension	Mbp1(124)	Mbp1(124):DNA complex
$<\tau(4–100)>$	ns	12.1±0.7	20.2±2.3
$<S^2(4–100)>$		0.91±0.06	0.87±0.07
Anisotropy		1.85(1.6–2)	2.4 (2.1–2.7)
$<J(0)(4–100)>=<\tau_0>$	ns	11.3±1.2	18.3±3.2
$<\tau(N)$ (4–100)>	ns	13.2±0.8	22.6±1.6
$<\tau(H)$ (4–100)>	ns	9.3±3.0	15.3±9

$<\tau_0(4–100)>$ is the averaged global correlation time for the Lipari–Szabo molecule using core residues 4 to 100 and $<S^2(4–100)>$ is the corresponding averaged order parameter. Anisotropy (range) was calculated from the fitting procedure as described in the text. $<J(0)(4–100)>$ is the averaged value of J(0) over residues 4–100. $<\tau(N)(4–100)>$ and $<\tau(H)$ (4–100)> are the apparent correlation times averaged over these residues as calculated from the spectral densities at ω_N and ω_H, respectively (see text).

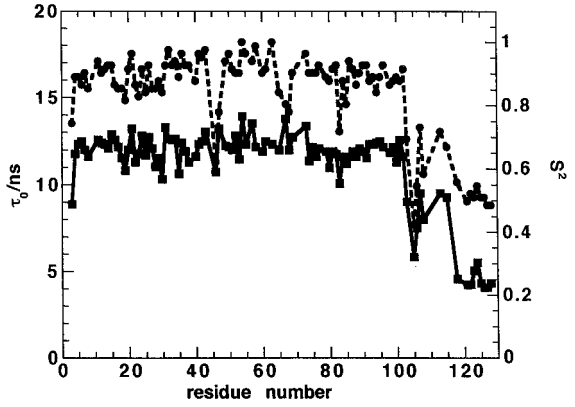

Figure 5. Rotational correlation times and order parameters for free Mbp1(124) at 288 K. τ_0 and S^2 were determined from the relaxation rate constants measured at 11.75 and 14.1 T as described in the text. (■ —) τ_0; (● —) S^2 from the global (11.75 T + 14.1 T) data.

order parameters of the majority of these residues are 0.91±0.06 (Table 1), also typical of backbone NH in structured proteins (Kay et al., 1989; Barbato et al., 1990; Clore et al., 1990; Kördel et al., 1992; Luginbühl et al., 1997; van Heijenoort et al., 1998). A small number of residues in the wing (Figure 1) of the protein show significantly lower order parameters, though the same correlation time (Figure 5), indicating that this region adjacent to the recognition helix has rather complex dynamics.

Errors in the motional parameters were estimated by synthesising 248 data sets with R_1, R_2 and NOE values corresponding to experimental values, to which Gaussian-distributed noise was added with a width equal to the experimental variance. For core residues, the standard deviation of τ_0 was 1.8% of the mean, with a range of about 0.5 ns on either side of the mean. The standard deviation of S^2 was 0.06, with a range of 0.03 on either side of the mean. Thus, for good quality relaxation data, the values of the site correlation time and order parameter can be expected to be well determined. The same is not true of the internal correlation time τ_e, where the error was almost as large as the mean value, as has been generally observed in other studies. The precision of the site correlation times and order parameters for residues in the tail were slightly less well determined, with standard deviations of around 5% of the mean.

The value of the site correlation times τ_0 for the core residues ranged from 14.5 ns to 10 ns (Figure 5). This range exceeds the experimental errors, implying that the molecular re-orientation is anisotropic. From the ratio of the maximum to the minimum τ_0 values (residues 4–102) (Schurr et al., 1994; Luginbühl et al., 1997), the correlation times for rotation of the long (τ_L) and short (τ_s) axes were calculated, from which $\tau_s \cong 8$ ns; this indicates an anisotropy of approximately 2. The data were then re-analysed using the anisotropic rotor model with several different values of τ_L and the anisotropy in a range of ±50% of these initial estimates. Excellent agreement was obtained for τ_L in the range 14–15 ns, and with $\tau_s = 8$–9 ns, and a best anisotropy of 1.8 (Table 1). This gave an overall improved agreement with the data for the core residues. However, the most C-terminal residues (117 onwards) still showed significant errors for anisotropies up to 4 (not shown), which indicates that such a simple model cannot adequately account for a coil region that can re-orient essentially independently of the core.

Using the co-ordinates derived from the X-ray structure, we calculated the principal components of

the moment of inertia tensor for the core of the protein, which shows an anisotropy of ca. 1.5:1. However, this degree of anisotropy cannot be used to calculate the rotational anisotropy that is probed by the ^{15}N NMR relaxation experiments, because it does not include the viscous drag generated by the structured part of the tail and the various interconverting conformations of the extensive tail region. Therefore, the anisotropy observed by NMR relaxation is not necessarily the same as the anisotropy calculated from the X-ray structure. The angle θ that each N-H vector makes with the principal axis of the diffusion tensor was also calculated. Because the dependence of the relaxation rate constants on θ is rather weak for modest anisotropy (τ_L/τ_S ca. 2), these angles are not determined with high precision. This has been confirmed using simulated data which demonstrate that even with small experimental uncertainties in the relaxation parameters, the values of θ that are recovered are quite imprecise when the order parameters and internal correlation times are also allowed to vary. The R_2/R_1 ratios for core residues were analysed as described by Clore et al. (1999), indicating an oblate ellipsoid, with a principal axis nearly perpendicular to the beta sheet structure (cf. Figure 1). This is in moderate agreement with that calculated from the X-ray structure.

Figure 5 clearly shows that for residues 102–107 and 117 onwards, the apparent site correlation times decrease to ca. 4–6 ns and the order parameters decrease to ca. <0.6, indicating that these residues undergo large-amplitude rapid motions with respect to the core of the protein.

Spectral density mapping

We have derived the spectral densities as described in the Methods. Figure 6 shows the values of J(0), J(ω_N) and J(ω_H) for each NH in the free protein. The value of J(0) shows the same variation along the sequence as τ_0 determined using the Lipari–Szabo model (see above), except that the value of J(0) is slightly smaller. As expected, J(ω_H) and J(ω_N) are much smaller than J(0). J(ω_N) is essentially constant for residues 4–110, and increases to a plateau value beyond residue 120. J(ω_H) is also almost constant between residues 4 and 102. There is then an increase from residue 103 onwards, apart from a minimum at residue 114, before finally reaching a plateau value by residue 120. J(ω_H) therefore closely follows the behaviour of J(0) except that the directions of the changes are opposite. This variation of the spectral densities at the three frequencies clearly shows the overall increase in mobility beyond

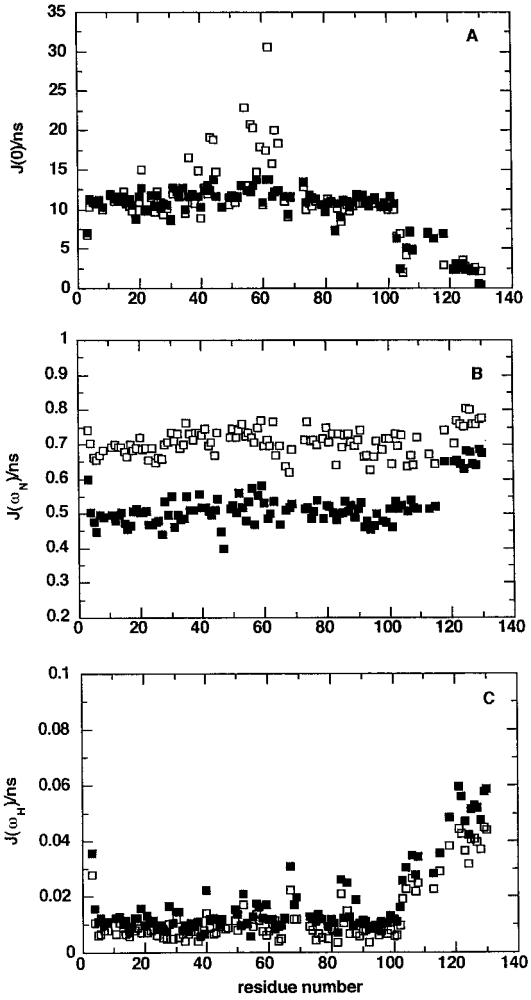

Figure 6. Spectral densities in free Mbp1(124) at 288 K. Spectral densities J(0), J(ω_N) and J(ω_H) were determined as described in the text. (A) J(0) calculated for data including (□) and excluding (■) the exchange contribution. (B) J(ω_N) at 50 (□) and 60 (■) MHz. (C) J(ω_H) at 500 (□) and 600 (■) MHz.

the core of the protein, and also the structuring (lower mobility) near residue 110.

Once a spectral density value has been determined, it is possible to calculate apparent correlation times for the NH vectors from each spectral density using the rigid-sphere correlation function $J(\omega) = \tau/(1 + \omega^2\tau^2)$. If the molecule does behave as a rigid sphere then the correlation times should be the same for each spectral density function and at each site. However, for Mbp1(124), the correlation times calculated from J(0), J(ω_N) and J(ω_H) are not equal, but lie in order $\tau(\omega_N) > \tau(0) > \tau(\omega_H)$ (Table 1): this requires that there must be at least one motion that contributes to relaxation in addition to that of isotropic overall

Table 2. Correlation times and amplitudes derived from the spectral densities of Mbp1(124)

Region	n	a_1	τ_1 (ns)	a_2	τ_2 (ns)	χ^2
Free						
4–100	1	1.0	11.0	–	–	0.031
	2	0.90	12.2	0.10	0.045	1.69 E–5
102–108	1	1.0	4.57	–	–	1.096
	2	0.58	7.53	0.42	0.057	4.19 E–4
109–116	1	1.0	7.43	–	–	0.32
	2	0.73	9.97	0.27	0.091	1.58 E–4
121–129	1	1.0	2.45	–	–	0.48
	2	0.51	4.67	0.49	0.092	2.2 E–3
Complex						
4–100	1	1.0	19.1	–	–	0.009
	2	0.91	20.9	0.09	0.042	4.9 E–5
121–129	1	1.0	4.7	–	–	0.96
	2	0.59	7.66	0.41	0.12	0.004

Correlation times, τ_i, and amplitudes a_i were determined using Equation 7 for different values of n. Quantitative analysis of the residues 102–108 and 109–118 in the complex was not attempted owing to insufficient data to average.

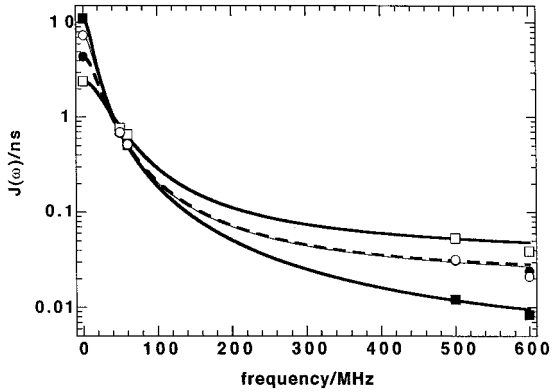

Figure 7. Spectral density functions of free Mbp1(124). Spectral densities at 0, 50, 60, 500 and 600 MHz were obtained as described in the text. Values were averages: core (4–100) (■), random coil segment of the tail (121–130) (□), the tail loop (102–107) (●) and the tail structured portion (109–116) (○). The spectral density function was fitted to Equation 7 with n = 2.

tumbling. In the C-terminal tail, the spectral densities are very different from those found in the core, as is reflected by the much lower apparent correlation times. This implies the presence of substantial amplitude motions on a shorter time-scale.

The spectral density functions at the different frequencies sampled (0, 50, 60, 500 and 600 MHz) show that for all residues that have no exchange contributions at kHz frequencies, the dominant motion is either 10–14 ns (core) or 2–5 ns (tail), with higher frequency motions accounting for only a small amount of relaxation for the core residues, but a significant fraction of the relaxation in the mobile tail residues. Figure 7 shows the spectral densities at 0, 50, 60, 500 and 600 MHz for core, random coil regions in the tail (residues 121–130), loop (102–108) and the structured region of the tail (109–116). For a rigid sphere, the spectral density function is expected to show a simple Lorentzian dependence on the frequency. In fact, a single Lorentzian does not account for any of the regions of the protein. The core residues are well represented by two Lorentzians, with amplitudes of 0.9 and 0.1 for correlation times of 14 ns and 44 ps (Figure 7, Table 2). These values are essentially identical to those found for the Lipari–Szabo analysis, indicating that on average, the core can be described by two uncoupled dynamic processes. As we have used the average over the core residues, the anisotropy has been averaged out. In contrast, the other three regions show different amplitudes at zero frequency, and at highest frequency deviate slightly from the two-Lorentzian fit. This indicates that different motions affect these residues at both low frequency and at very high frequency. Overall, the ^{15}N relaxation of Mbp1(124) shows complex motional behaviour with anisotropic overall rotation of the molecule, fast dynamics in a loop and the C-terminal part of the tail, and slow exchange dynamics in the two regions flanking the recognition helix.

Relaxation behaviour of the Mbp1(124)-DNA complex

Relaxation data were acquired at 11.75 T and 14.1 T for the Mbp1(124):DNA complex as described for the free protein (Figure 8). Owing to the much faster spin-spin relaxation and the consequent decrease in resolution and sensitivity, the scatter of the R_2 data in particular is larger than for the free protein. However, independent estimates of R_2 from repeated CPMG experiments, $R_{1\rho}$ and ^{15}N line widths (see Methods) showed that the variation of rate constants along the sequence was reproducible. The pattern of relaxation rate constants in the tail compared with the core is similar to that observed in the free protein, suggesting that similar conformational and dynamic properties are preserved in the complex. Residues 102–108 and those beyond residue 120 remain highly mobile. As for the free protein, there is a group of residues (109–120) that have relaxation rate constants intermediate between those in the core and the other tail residues. This indi-

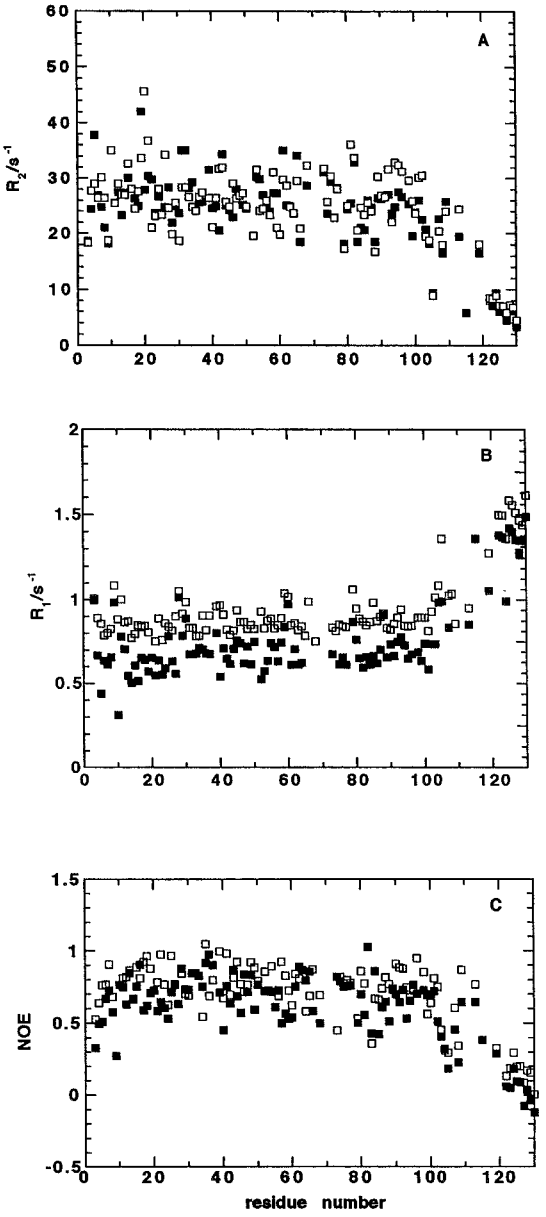

Figure 8. Relaxation rate constants in the Mbp1(124):DNA complex at 288 K. ^{15}N relaxation rate constants were determined at 11.75 and 14.1 T as described in the text. (A) R_2 at 14.1 T (■) and 11.75 T (□). (B) R_1 at 14.1 T (■) and 11.75 T (□). (C) NOE (●) at 14.1 T and (○) 11.75 T.

cates the presence of a structured region within the tail, which is slightly more extended in the protein:DNA complex. The NOEs between Ala 114 and Ser 6 and Tyr 7 observed in the free protein are maintained in the complex, indicating that the same structural feature is present in both states of the protein.

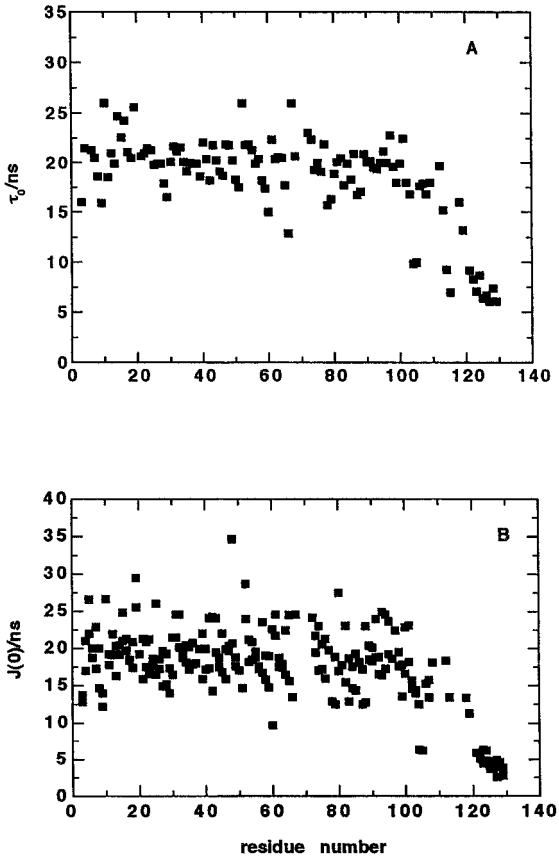

Figure 9. Correlation times and spectral densities in the Mbp1(124):DNA complex at 288 K. (A) τ_0 averaged over the data from 11.75 T and 14.1 T. (B) J(0) averaged over the data from 11.75 T and 14.1 T.

The average rotational correlation time determined from the Lipari–Szabo analysis was 20.2±2.3 ns for the core residues, which is ca. 1.7-fold larger than for the free protein (Table 1). The increase in the average rotational correlation time correlates with the increase in molecular volume due to binding the DNA duplex (Mr = 7800). The mean order parameter for the core residues was 0.87±0.07, which is not significantly different from the average value found in the free protein (Table 1). Similarly, the order parameters and correlation times for residues 120 onwards in the complex are similar to those in the free protein (Figures 5 and 9). This strongly suggests that there are no direct long-lived contacts between the final C-terminal residues and the DNA. The variation of τ_0 within the core indicates that the complex also reorients anisotropically. From this variation, we estimate an apparent anisotropy of ca. 2–2.4 for the complex, which is slightly larger than observed for the free protein (Ta-

ble 1). As for the free protein, using an anisotropic rotor model improves the overall agreement with the data, with the exception of the terminal residues which require a much smaller correlation time.

None of the residues that showed slow conformational exchange (40–45, 56–64) in the free protein had anomalously high R_2 values in the protein:DNA complex (cf. Figures 2 and 8). This could arise from several effects: a shift in the equilibrium so that only one conformation is populated, the ^{15}N frequency difference between the conformational states decreased in the complex, or because the exchange rate constant is greatly increased in the complex. The last possibility seems improbable, as a decrease in the exchange rate constants in the complex would be expected, owing to the general tightening of the protein. It is more likely that the DNA binds one form more tightly than the other, altering the equilibrium, and possibly also the relative shift difference. Significant changes in ^{15}N shifts do occur in this (and other) regions of the protein (McIntosh et al., 1999), which also suggests a stabilisation of one state over the other. These residues have been implicated in the binding surface by virtue of structural homology with related DNA-binding proteins, the electrostatic potential (Taylor et al., 1997), and chemical shift mapping (Taylor et al., 2000).

The pattern of spectral densities found for the complex is qualitatively similar to that of the free protein. The apparent correlation times calculated from the three spectral densities are not equal but lie in the order $\tau(\omega_N) > \tau(0) > \tau(\omega_H)$, as for the free protein, indicating that dynamics of the core should not be described by a single correlation time. The spectral densities of the core can be fitted to a sum of two Lorentzians (Table 2) that are essentially identical to those obtained from the Lipari–Szabo analysis. However, the random-coil tail residues show substantially higher mobility than the core, as demonstrated by their having a higher amplitude for the short correlation-time motion, together with a smaller amplitude and lower value for the component with the longer correlation time. Qualitatively, the loop and structured residues show the same behaviour as in the free protein. However, the quantitative analysis was not attempted owing to the relative paucity of data in this region.

Discussion

Mbp1(124) shows a rich ^{15}N relaxation behaviour resulting from motions on very short time scales ($<$ 200 ps) with order parameters of ca. 0.9, larger amplitude motions on the 2–5 ns time scale, global rotational motions on the 8–14 ns time scale and much slower processes on the ms time scale. The richness of the motions requires complex mixtures of spectral density functions to describe all of the relaxation. Slow conformational exchange was found for residues in the loop between helix A and the putative recognition helix B, and at the end of helix B extending into the adjacent loop and β strand 5 (Figure 1). Interestingly, the relaxation properties of the tail residues indicated that in solution it folds back onto the core of the protein. This was confirmed by the observation of NOEs between Ala 114 in the tail and residues in the first β sheet of the protein (Figure 3). Residues C-terminal to Phe100 were not observed in the crystal structure; no doubt this is in part due to the dynamic disorder of the tail residues. Only a small number of NOEs were observed between tail and beta strand residues, and according to the relaxation data (Figures 2 and 8), $<$10 residues in the tail might be ordered due to this interaction. This suggests a relatively weak interaction that could be displaced by crystal packing interactions.

The main effects of DNA binding are decreased overall rotation, as expected for an approximately 60% increase in size, and quenching of most of the ms motions, i.e. those adjacent to the putative DNA recognition helix (Figure 1). The formation of the Mbp1(124):DNA complex affected the dynamics of only a few residues in the tail, increasing the structured region from ca. residue 117 to 120. This may account for the observed changes in N and H^N chemical shifts of residues 119–121 on binding DNA (McIntosh et al., 1999). This indicates that the entropy cost of DNA binding from ordering the tail is small, in contrast to FruR, where a more extensive organisation of tail residues was reported (van Heijneoort et al., 1998). Recently Feher and Cavanagh (1999) have observed a localised region of the protein Spo0F that has a large exchange contribution to J(0), and which correlates with the binding to other proteins. This kind of millisecond dynamics in protein backbones may be fairly common, and be involved in the recognition process, though the precise functional implications of the dynamics per se remain unclear. Nevertheless, this work shows a clear demonstration of a conformational selection related to the function of the protein.

Other winged helix-turn-helix proteins have been examined by NMR recently. Based on NH chemical shift changes, the second helix in the HtH motif in IRF-2 was proposed to interact in the major groove of the DNA, and a loop between a β strand and the first of the HtH helices might interact with the minor groove (Furui et al., 1998). In the Genesis winged HtH protein, ^{15}N relaxation experiments (Jin et al., 1998) indicated fast motions (reduced NOE and R_2 values compared with the core of the protein) in the two 'wing' regions in the C-terminal domain of the protein. In addition, slow conformational dynamics (ms time scale) were observed both in the region just N-terminal to the HtH motif, and within the putative recognition helix itself, which was interpreted as being due to collective slow dynamics. More recently, Jin and Liao (1999) have shown that the Lipari–Szabo model does not provide a complete description of the motions, and that the dynamics are complex. Furthermore, they showed that there is different temperature dependence to the dynamics in the protein–DNA complex. However, Mbp1(124) differs from these proteins in that it contains an additional two helices C-terminal to the β5 loop β6 structure (wing1, Figure 1), and the dynamically disordered C-terminal tail region. Thus the dynamics and presumed mode of binding to DNA of the wHTH class of proteins can vary significantly, reflecting the evolution of specific DNA binding mechanisms associated with homologous proteins within this family.

Acknowledgements

This work was supported by the Medical Research Council of the U.K. NMR experiments were carried out at the MRC Biomedical NMR Centre, Mill Hill. We thank Dr. Mark Carr for additional experiments at 14.1 T at the University of Kent. We thank Dr. Andrew Atkinson for discussions about spectral density mapping, and Dr. James Feeney for encouragement and support.

References

Barbato, G., Ikura, M., Kay, L.E., Pastor, R.W. and Bax, A. (1992) *Biochemistry*, **31**, 5269–5278.

Bax, A., Ikura, M., Kay, L.E., Torchia, D.A. and Tschudin, R. (1990) *J. Magn. Reson.*, **86**, 304–318.

Bodenhausen, G. and Ruben, D.J. (1980) *Phys. Lett.*, **175**, 477–482.

Bork, P. (1993) *Proteins*, **17**, 363–374.

Boyd, J., Hommel, U. and Campbell, I.D. (1990) *Chem. Phys. Lett.*, **175**, 477–482.

Breeden, L. and Nasmyth, K. (1987) *Nature*, **329**, 651–654.

Broadhurst, R.W., Hardman, C.H., Thomas, J.O. and Laue, E.D. (1995) *Biochemistry*, **34**, 16608–16617.

Clore, G.M., Driscoll, P.C., Wingfield, P.T. and Gronenborn, A.M. (1990) *Biochemistry*, **29**, 7387–7401.

Clore, G.M., Gronenborn, A.M., Szabo, A. and Tjandra, N. (1998) *J. Am. Chem. Soc.*, **120**, 4889–4890.

Daragan, V.A. and Mayo, K.H. (1997) *Prog. NMR. Spectrosc.*, **31**, 61–105.

Davis, D.G., Perlman, M.E. and London, R.E. (1994) *J. Magn. Reson.*, **B104**, 266–275.

Deverell, C., Morgan, R.E. and Strange, J.H. (1970) *Mol. Phys.*, **18**, 553–559.

Farmer, B.T., Macura, S. and Brown, L.R. (1988) *J. Magn. Reson.*, **80**, 1–22.

Farrow, N.A., Zhang, O., Szabo, A., Torchia, D.A. and Kay, L.E. (1995) *J. Biomol. NMR*, **6**, 153–162.

Feher, V.A. and Cavanagh, J. (1999) *Nature*, **400**, 289–293.

Fesik, S.W. and Zuiderweg, E.R.P. (1988) *J. Magn. Reson.*, **78**, 588–593.

Fischer, M.W.F., Majumdar, A. and Zuiderweg, E.R.P. (1998) *Prog. NMR. Spectrosc.*, **33**, 207–272.

Foord, R., Taylor, I.A., Sedgwick, S.G. and Smerdon, S.J. (1999) *Nat. Struct. Biol.*, **6**, 157–165.

Furui, J., Uegaki, K., Yamazaki, T., Shirakawa, M., Swindells, M.B., Harada, H., Taniguchi, T. and Kyogoku, Y. (1998) *Structure*, **6**, 491–500.

Jin, C., Marsden, I., Chen, X. and Liao, X. (1998) *Biochemistry*, **37**, 6179–6187.

Jin, C. and Liao, X. (1999) *J. Mol. Biol.*, **292**, 641–651.

Kay, L.E., Nicholson, L.K., Delaglio, F., Bax, A. and Torchia, D.A. (1992) *J. Magn. Reson.*, **97**, 359–375.

Kay, L.E., Torchia, D.A. and Bax, A. (1989) *Biochemistry*, **28**, 8972–8979.

Koch, C., Moll, T., Neuberg, M., Ahorn, H. and Nasmyth, K. (1993) *Science*, **261**, 1551–1557.

Kördel, J., Skelton, N.J., Akke, M., Palmer, A.G. and Chazin, W.J. (1992) *Biochemistry*, **31**, 4856–4866.

Kraulis, P. (1991) *J. Appl. Crystallogr.*, **24**, 946–950.

Lane, A.N., Bauer, C.J. and Frenkiel, T.A. (1993) *Biophys. J.*, **21**, 425–431.

Lefèvre, J.F., Dayie, K.T., Peng, J.W. and Wagner, G. (1996) *Biochemistry*, **35**, 2674–2686.

Levy, R.M., Karplus, M. and Wolynes, P.G. (1981) *J. Am. Chem. Soc.*, **103**, 5998–6011.

Lipari, G. and Szabo, A. (1982) *J. Am. Chem. Soc.*, **104**, 4546–4559.

Lowndes, N.F., Johnson, A.L., Breeden, L. and Johnston, L.H. (1992) *Nature*, **357**, 505–508.

Luginbühl, P., Pervushin, K.V., Iwai, H. and Wüthrich, K. (1997) *Biochemistry*, **36**, 7305–7312.

McIntosh, E.M., Atkinson, T., Storms, R.K. and Smith, M. (1991) *Mol. Cell Biol.*, **11**, 329–337.

McIntosh, P.B., Taylor, I.A., Frenkiel, T.A., Smerdon, S.J. and Lane, A.N. (1999) *J. Biomol. NMR*, **13**, 397–398.

Peng, J.W. and Wagner, G. (1992) *J. Magn. Reson.*, **98**, 308–332.

Press, W.H., Flannery, B.P., Teukolsky, S.A. and Vetterling, W.T. (1986) Numerical Recipes. The Art of Scientific Computing, Cambridge University Press, Cambridge, ch. 14.

Primig, M., Sockanathan, S., Auer, H. and Nasmyth, K. (1992) *Nature*, **358**, 593–597.

Schurr, J.M., Babcock, H.P. and Fujimoto, B.S. (1994) *J. Magn. Reson.*, **B105**, 211–224.

Schwalbe, H., Fiebig, K.M., Buck, M., Jones, J.A., Grimshaw, S.B., Spencer, A., Glaser, S.J., Smith, L.J. and Dobson, C.M. (1997) *Biochemistry*, **36**, 8977–8991.
Sedgwick, S.G., Taylor, I.A., Adam, A.C., Spanos, A., Howell, S., Morgan, B.A., Treiber, M.K., Kanuga, N., Banks, G.R., Foord, R. and Smerdon, S.J. (1998) *J. Mol. Biol.*, **281**, 763–775.
Sedgwick, S.G. and Smerdon, S.J. (1999) *Trends Biochem.*, **24**, 311–316.
Sidorova, J. and Breeden, L. (1993) *Mol. Cell. Biol.*, **13**, 1069–1077.
Szyperski, T., Luginbühl, P., Otting, G., Güntert, P. and Wüthrich, K. (1993) *J. Biomol. NMR*, **3**, 151–164.
Taylor, I.A. and Smerdon, S.J. (1997) *Proteins*, **27**, 325–327.
Taylor, I.A., Treiber, M.K., Olivi, L. and Smerdon, S.J. (1997) *J. Mol. Biol.*, **272**, 1–8.
Taylor, I.A., Pala, P., McIntosh, P.B., Lane, A.N. and Smerdon, S.J. (2000) *Biochemistry*, in press.
Tjandra, N., Feller, S.E., Pastor, R.W. and Bax, A. (1995) *J. Am. Chem. Soc.*, **117**, 12562–12566.
Tjandra, N., Garrett, D.S., Gronenborn, A.M., Bax, A. and Clore, G.M. (1997) *Nat. Struct. Biol.*, **4**, 443–449.
Van Heijenoort, C., Penin, F. and Guittet, E. (1998) *Biochemistry*, **37**, 5060–5073.
Wand, A.J., Urbauer, J.L., McEvoy, R.P. and Bieber, R.J. (1996) *Biochemistry*, **35**, 6116–6125.
Wishart, D.S., Sykes, B.D. and Richards, F.M. (1992) *Biochemistry*, **31**, 1647–1651.
Wishart, D.S. and Sykes, B.D. (1994) *J. Biomol. NMR*, **4**, 171–180.
Woessner, D.E. (1962) *J. Chem. Phys.*, **37**, 647–654.
Xu, R.M., Koch, C., Liu, Y., Horton, J.R., Knapp, D., Nasmyth, K. and Cheng, X. (1997) *Structure*, **5**, 349–358.
Yang, D. and Kay, L.E. (1996) *J. Mol. Biol.*, **263**, 369–382.
Zheng, Z., Czaplicki, J. and Jardetzky, O. (1995) *Biochemistry*, **34**, 5212–5223.